Solar Energy Materials & Solar Cells 95 (2011) 765–772

Contents lists available at ScienceDirect

Solar Energy Materials & Solar Cells

journal homepage: www.elsevier.com/locate/solmat

The potential of sonicated water in the cleaning processes of silicon wafers

A. Podolian [a], A. Nadtochiy [a], V. Kuryliuk [a], O. Korotchenkov [a,*], J. Schmid [b], M. Drapalik [b], V. Schlosser [b]

[a] Faculty of Physics, Taras Shevchenko Kyiv National University, Kyiv 01601, Ukraine
[b] Department of Electronic Properties of Materials, Faculty of Physics, University of Vienna, A-1090 Wien, Austria

ARTICLE INFO

Article history:
Received 7 September 2010
Accepted 19 October 2010
Available online 19 November 2010

Keywords:
Silicon wafers
Cleaning
Sonication
Photovoltaic

ABSTRACT

The potential of using distilled water in environmental friendly and non-toxic ultrasonic cleaning step in crystalline Si wafer preparation is addressed. It is found that organic particle contaminants are effectively removed during the kHz-frequency sonication of wafers over the first 40–60 min, as evidenced by the disappearance of organic-related optical absorption peaks. Subsidiary effects of the sonication on electrical and photoelectrical behaviour of Si wafers are discussed. It is observed that, when treating the wafers less than 60 min, the dangling bonds at the air/oxide and oxide/wafer interface can be activated. That causes a decrease in the subsurface resistance against dislocation displacements (observed microhardness decrease). It affects barriers of the free carrier migration at the interfaces (revealed in the current–voltage characteristics), and acts as recombination centers, accelerating photovoltage decays. A healing of the bonds may occur at longer cleaning times ($\approx$ 60–120 min), which partially recover the interfaces, thus reversing the observed changes. Although an exact mechanism is not yet clarified, the likely scenario behind the observed changes is proposed to involve oxygen and hydrogen molecules, which are decomposed in water and subsequently trapped at the silicon surface.

1. Introduction

As silicon device technology in the photovoltaic and microelectronic industries progresses, a good control of physico-chemical properties of ultraclean wafer surfaces and Si/SiO_2 interfaces are required. Thus, clean substrate surfaces are crucial in high-efficiency solar cell as well as in the ultra-large scale integration (ULSI) fabrication processes for obtaining maximum device performance, long-term reliability, and high yields. The rapid increase in processed wafers together with an increase in the number of cleaning sequences raise the demand for new safe and economical cleaning solutions. A 64 Mb 0.25 μm dynamic random access memory (DRAM) manufacturing process has up to 70 cleaning steps. About 80 of the total 400 process steps in a 0.18 μm complementary metal oxide semiconductor (CMOS) technology are cleaning steps [1]. Wafer preparation for deposition of monolayers and self-assembly of nanoparticles requires the surface to be completely free of any particulate contamination down to a nanometer scale. To install a photovoltaic power generator with 1 MW_p about 250 000 silicon wafers with 156 mm edge length must be processed.

Modern wafer manufacturing facilities use various methods of cleaning wafers, which involve pressurized water jet scrubs, rotating wafer scrubbers, wet chemical baths and rinses, etc. These processes, however, are prone to damaging the wafer. In addition, the chemical processes have inherent dangers associated with the use of chemicals, such as sulfuric acid, ammonium hydroxide, and isopropyl alcohol. In this context, a substrate-independent cleaning process is highly desirable because, opposite to a chemical-based cleaning process, it is equally well suited for different substrates and does not modify the surface through the etching, roughening, etc.

The surface contamination of wafers by particle contaminants is one of the major problems in the industries. One way to increase the yield on fully processed silicon wafers is to use cleaning techniques specifically efficient to remove particle contaminants. Small particles are especially difficult to remove because they are strongly bound to the substrate by electrostatic forces. It is therefore very important to find an effective way to remove particles from wafers without causing damage to the wafers.

In order to meet the International Technology Roadmap for Semiconductors requirements [2] and to resolve the concerns raised, ultrasonic cleaning processes can be used. Ultrasonic cleaning involves a variety of complex mechanisms, including mechanical vibration and appropriate pressure gradients [3], microcavitation bubbles that oscillate and dance around due to Bjerknes force [4], acoustic streaming flows [5], etc., depending on whether liquids are used in the cleaning process or not. In a liquid-filled ultrasonic bath, a typical ultrasonic source is a plane surface attached to the bath flask that oscillates at a single frequency f and produces a longitudinal wave. Acoustic energy is then transmitted to the wafer by the wave, which propagates through the fluid. One

* Corresponding author.
E-mail address: olegk@univ.kiev.ua (O. Korotchenkov).

0927-0248/$ - see front matter © 2010 Elsevier B.V. All rights reserved.
doi:10.1016/j.solmat.2010.10.019

of the most important aspects of using acoustic streaming is the effect of the frequency on the boundary layer. The thickness of the acoustic boundary layer decreases with increase in the frequency, and the streaming velocity increases. Both effects tremendously increase the drag force and consequently the particle removal moment. When the applied removal moment overcomes the adhesion moment, removal will take place. It is demonstrated that the removal of nano-size particles (10–100 nm) can be accomplished using acoustic streaming at frequencies greater than 1 MHz (typically referred to as high-frequency megasonics) [6]. Experimental results show that complete removal down to 100 nm is possible using frequencies lower than 1 MHz [7]. Despite well-established observations of the cleaning of immersed surfaces, the physical explanation of how the particles are removed is still subject to debate [8].

Thus, the removal of more than 99% of silica and silicon nitride from silicon substrates using megasonics in deionized water and SC1 ($H_2O/H_2O_2/NH_4OH$: 40/2/1) solution was reported [9].

It was reported that the presence of the ultrasonic wave in the caustic etching process enhances the etching rate and results in a finer, and more homogeneous, textured structure [10]. This allows enhancing the solar cell performance inhibiting reflection of irradiated sunlight by the silicon surface. The texture, etched for 20 min at 60 °C in the caustic solution with ultrasonic excitation gives higher cell performance than the cell texture etched for 40 min at 70 °C without ultrasonic wave. This indicates a possibility of lowering the texturing cost by saving time and expensive chemicals normally employed in the texturisation of the crystalline silicon.

In this work, the wafer cleaning and deterioration effects were investigated in distilled water and piranha (3:1 volume solution of H_2SO_4 and 30% H_2O_2) as a function of the cleaning time (0–120 min) using current–voltage (I–V) characteristics, surface photovoltage (SPV) decays and micro-hardness (HV) measurements.

It is therefore our intention to present a few considerations on the basic features and potential of the cleaning procedure that can be further evaluated towards an environmental friendly cleaning step in Si wafer preparation. We hope that these considerations will stimulate a new thinking about wafer cleaning by employing a cheap sonication in distilled water. Current challenges and future prospects are outlined. This study is aimed at developing a low-cost and environmental friendly cleaning of bare silicon wafers with the aid of ultrasonic energy.

2. Experimental details

An overview of the ultrasonic apparatus is shown in Fig. 1. An oscillating voltage with the amplitude of U_0 applied to a Langevin transducer causes it to vibrate, thus delivering an acoustic power into the water (or piranha)-filled flask at the transducer-solution system's resonance frequency. The resonance frequency is defined by the water thickness h. In our experiments, it was adjusted to the resonant frequency of the unloaded transducer of 28 kHz, such that h is taken to be about $\lambda/2$ with λ the sound wavelength in water at the resonant frequency. The temperature of the bulk water was kept between 70 and 80 °C during the entire treatment. In the geometry of Fig. 1, a cavitation is readily observed at $U_0 \geq 45$ V. The silicon wafer was not fixed in the bath flask, so that different values of the incident angle are realized for the traveling acoustic wave.

2.1. Estimating acoustic power and wave characteristics

For an acoustic power analysis as well as for a better understanding of measured variables, it is important to introduce

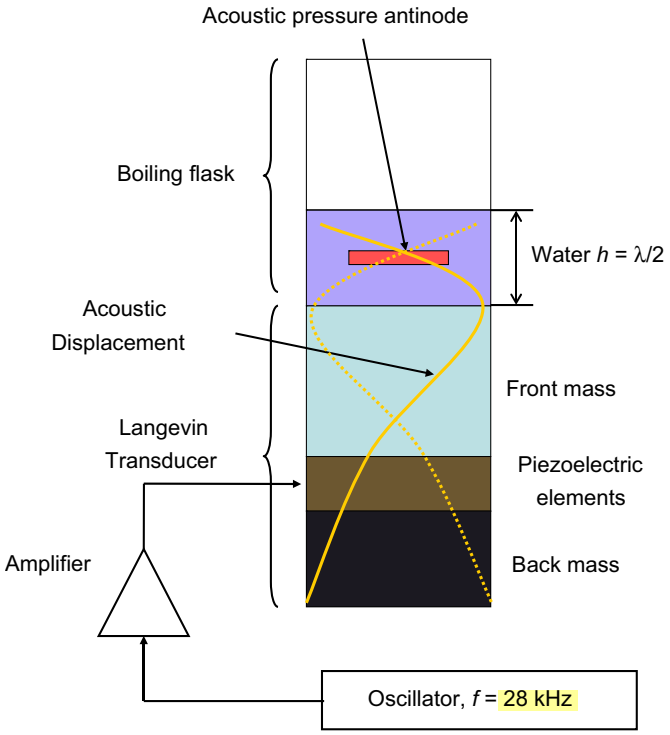

Fig. 1. Schematic of the experimental apparatus for sonication of wafers (not to scale).

parameters of the transducer and a quality factor of the transducer–water system as a whole. The Langevin transducer has a composite structure, as sketched in Fig. 1. It is assembled from two or more piezoelectric elements, back steel mass and front aluminium mass. Despite the composite structure, the Langevin transducer can be characterized by introducing an equivalent electrical circuit for a conventional piezoelectric transducer operating at a frequency of the natural resonance shown in Fig. 2 [11]. The capacitor C_t represents the shunt capacitance that includes the metal electrodes deposited onto the transducer surface, holder and leads. The R_S–L_S–C_S element composes the motional arm of the transducer with the resistance R_S accounting for the bulk losses occurring within the piezoelectric body, the motional inductance L_S representing the vibrating mass of the transducer and the motional capacitance reflecting the piezoelectric body elasticity.

The equivalent circuit for a piezoelectric transducer in water is modified by introducing additional elements shown in Fig. 2(b). They include the motional inductance (L_{water}) and resistance (R_{water}) terms reflecting the mass loading and acoustic energy dissipation, respectively. They also include the inductance L_m, which is due to the mass loading resulting from likely adsorption of species from the water.

The admittance spectrum of the Langevin transducer in the frequency range of interest is shown in Fig. 3. The main resonance at about 28 kHz shows the admittance maximum and minimum at two frequencies, f_{max} and f_{min}, respectively. These can be given in terms of the series resonant frequency, $f_r = 1/(2\pi\sqrt{L_S C_S})$, which is determined by the motional arm elements L_S and C_S neglecting losses due to energy dissipation. Then $f_{max} = f_r(1-\Delta)$ and $f_{min} = f_r(1+\Delta+C_S/2C_0)$, where $\Delta = C_t/(8\pi^2 C_S f_r^2 L_s^2/R_s^2)$, $C_0 = C_t + C_x$, and C_x is the parallel load capacitance (parallel to C_t, not shown in Fig. 2(b)). It is seen that f_{max} is very close to the resonant frequency f_r, whereas f_{min} is very close to $f_a = f_r(1+C_S/2C_0)$, often called the antiresonant frequency. Therefore, in what follows, we use $f_{max} \approx f_r$ and $f_{min} \approx f_a$.

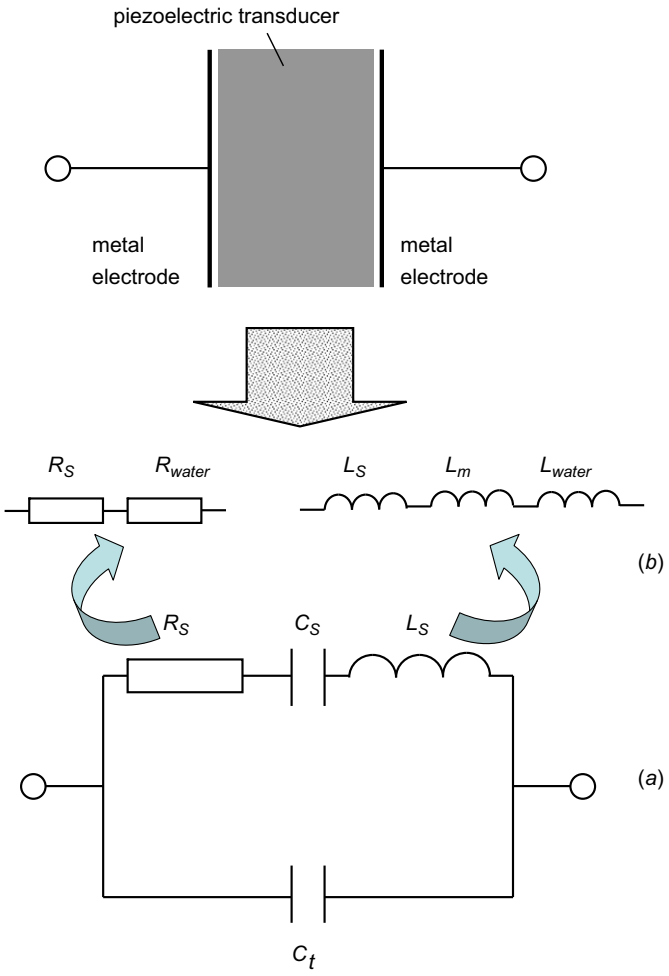

Fig. 2. Equivalent circuit for a conventional piezoelectric transducer operating at a frequency of the natural resonance when oscillating in air (*a*) and in water (*b*).

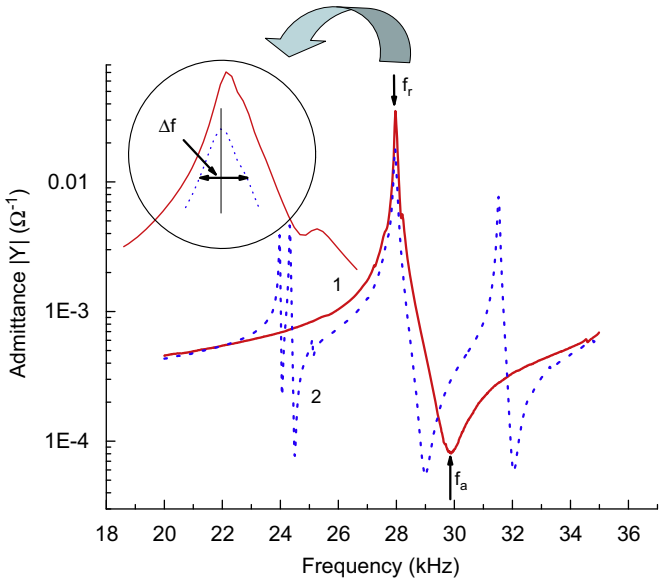

Fig. 3. Frequency dependence of the Langevin transducer admittance, air- (1) and water-loaded (2).

The relative quality, or efficiency of oscillations, is characterized by the quality factor *Q*. The sharper the admittance peak, the narrower the transducer bandwidth and the greater the value of *Q*, which can also be given by $Q=2\pi f_r L_S/R_S$. The Langevin transducer used here is specially designed for use in liquid-loaded systems, as evidenced by the fact that the admittance peak is only weakly affected by the water loading (curve 2 compared with curve 1 in Fig. 3). The quality factor can easily be estimated from the data of Fig. 3 as $Q=f_r/\Delta f$, where Δf is the half width of the admittance peak. It can also be estimated from $Q=\pi/\alpha\lambda$ with α the attenuation coefficient. In our experiments, $Q\approx 300$. The shunt capacitance is simply $C_t=Y_0/(2\pi f_0)$, where Y_0 is the admittance taken at a frequency f_0, which is much smaller than f_r.

From Fig. 3, the electromechanical coupling coefficient K_t is

$$K_t^2=\frac{\pi}{2}\frac{f_r}{f_a}\cot\left(\frac{\pi}{2}\frac{f_r}{f_a}\right). \tag{1}$$

Then the pressure amplitude of the incident wave with respect to the wafer surface can be found as

$$P_0=U_0\rho V\sqrt{\frac{K_t^2C_t}{M_t}}G(Q_1,Q_2), \tag{2}$$

where ρ is the water density, V the sound velocity in water, M_t the mass of the transducer and $G(Q_1,Q_2)$ a function that depends upon the acoustic losses in the transducer (Q_1) and water (Q_2). Analyzing vibrations of the two joining layers, one finds

$$G(Q_1,Q_2)=\frac{2ch^2(\pi/4Q_1)ch(\pi/4Q_2)}{2sh(\pi/2Q_1)ch(\pi/2Q_2)+nch(\pi/2Q_1)sh(\pi/2Q_2)}\approx\frac{2}{\pi}\frac{1}{(1/Q_1)+(n/2)(1/Q_2)}, \tag{3}$$

where n is the ratio of the acoustic impedances of water and the transducer $n=(\rho V)_{\text{water}}/(\rho V)_{\text{transducer}}$.

Taking $U_0=225$ V, $\rho=1000$ kg/m^3, $V=1500$ m/s, $M_t=0.4$ kg, $K_t^2=0.14$, $C_t=3.5$ nF and $G(Q_1,Q_2)=300$ for our experimental conditions, the pressure amplitude P_0 of 3.5 MPa is obtained. Then the peak acoustic intensity is

$$I=\frac{P_0^2}{2\rho V}, \tag{4}$$

which yields $I\approx 400$ W/cm^2. The wave amplitude A_0 can be simply related to P_0 as

$$\frac{P_0^2}{2\rho V}=\frac{1}{2}\rho V(2\pi f)^2A_0^2, \tag{5}$$

which readily gives $A_0=P_0/2\pi f\rho V=13$ μm at $P_0=3.5$ MPa.

2.2. Removing a contaminating material from the wafer surface

Some contaminants comprise insoluble particles loosely attached and held in place by ionic or cohesive forces. These particles need only be displaced sufficiently to break the attractive forces to be removed. Cavitation, implosion and acoustic streaming as a result of ultrasonic activity displace and remove loosely held contaminants, such as dust or organic substances from surfaces.

Approximating acoustic streaming effect, we may now estimate the stress exerted on the wafer surface by the ultrasonic wave. Suppose the normal force F_n, expressed in units of N/m, is due to the pressure difference between the solid and the fluid, and is nearly independent of the incidence angle and frequency. The reduced normal force, $F_n/2RP_0$, is then nearly equal to 1, where $2R$ is the bounding length of the contaminating particle/surface interface [12].

The tangential component of the reduced force depends strongly on frequency and incidence angle θ and can be approximated by a linear relationship of the form [12]

$$\frac{F_t}{2RP_0}=2\pi\alpha\frac{fR}{V} \tag{6}$$

with $\alpha=4.3587\ \sin\ (1.0538\theta-5.3733)+0.04097$, where θ is in degrees. This force is due to the pressure gradient across the contaminating particle in the passing acoustic wave. As the wavelength shortens, the pressure gradient increases thus leading to the increased tangential force.

Consider the contaminating features of 10 μm ($R=5$ μm) and take $\theta=90^\circ$ producing the maximum values of F_n and F_t [12]. Then $F_n \approx 35$ N/m and $F_t \approx 0.1$ N/m at $P_0=3.5$ MPa.

A contaminant particle adhering to the wafer surface may be removed if the force given by the F_n and F_t components counteracts the London–van der Waals adhesion force, usually considered to be the dominant attractive force for short distances in particle adhesion [13]. The van der Waals force of adhesion between a spherical particle of radius r_0 and a surface is given by

$$F_a = \frac{A_{132}\, r_0}{6\,(d-r_0)^2}, \tag{7}$$

where d is the distance of the center of the particle to the surface. The effective Hamaker constant, A_{132}, is a function of the material constituting the particle (material 1), the surface (material 2), and the medium surrounding the particle/surface system (material 3). Here we consider the case of a silica contaminant particle in water adhering to a wafer coated with a thin layer of silica. It may be assumed that the unknown Hamaker constant for contaminating particle–water–silicon is in the range of 10^{-20}–10^{-21} J [14]. In the case of a particle nearly in contact with the surface, the separation distance $d-r_0$ is only on the order of a few angstroms [15]. Taking $r_0 \sim 1$ μm, $d-r_0 \sim 0.5$ nm gives $F_a \sim 10^{-8}$–10^{-9} N, illustrating that the removal of the contaminating material from the wafer surface is feasible, since $F_n 2R \sim 35\times10^{-5}$ N and $F_t 2R \sim 10^{-6}$ N, both exceeding the adhesion force.

The tangential force F_t leads to a shear stress, which can be estimated by $\tau = F_t/2R$ [12] yielding the value of ≈ 0.01 MPa. This may damage the wafer if the acoustic shear stress exceeds the shear strength of silicon. Let us now estimate the shear strength of silicon. The theoretical tensile strength of a brittle material may be estimated by the relation $\sigma_{th} = \sqrt{\gamma E/a_0}$ [16] where γ is the surface energy, E the Young modulus and $a_0=0.23517$ nm is the interatomic spacing in silicon. The Young modulus E is 13×10^{10}, 17×10^{10} and 19×10^{10} Pa for the surface orientations of [1 0 0], [1 1 0] and [1 1 1], respectively. The surface energy of silicon also depends on the crystallographic orientation of the surface and is found to be 1.23, 1.51 and 2.13 J/m^2 for [1 1 1], [1 1 0] and [1 0 0] surfaces, respectively. Then $\sigma_{th} \approx 30$ GPa. The experimental strength is typically 2–3 orders of magnitude smaller than σ_{th} [12]. Thus, the rupture modulus for bending silicon was found to be between 68 and 343 MPa [17], whereas the shear strength of a material is $\approx$40% of the tensile strength [18]. Then the shear strength of silicon may be as high as a few tens of MPa. Next, the wafer subjected to a cyclic load may exhibit smaller values of σ_{th} due to fatigue. A previous estimate shows that the dynamic fatigue strength of silicon may be $\approx$50% of its static strength [12]. Meanwhile, this obviously remains much greater than the acoustic shear stress $\tau = F_t/2R \approx 0.01$ MPa estimated previously, illustrating that the surface damage effect is unlikely with the wafer cleaning due to acoustic streaming. However, the bubble implosion could provide the force capable of damaging the wafer subsurface region, as can be deduced from previous pressure modeling done by different works (see, e.g., Ref. [4]).

It is therefore suggested that the Vickers micro-hardness variations are capable of providing indirect information on the subsurface state through varying mechanical hardness. The fields of elastic tensions caused by cavitation treatments of the wafer surface would extend deep enough inside the wafer to affect both the air/oxide and oxide/wafer interface states.

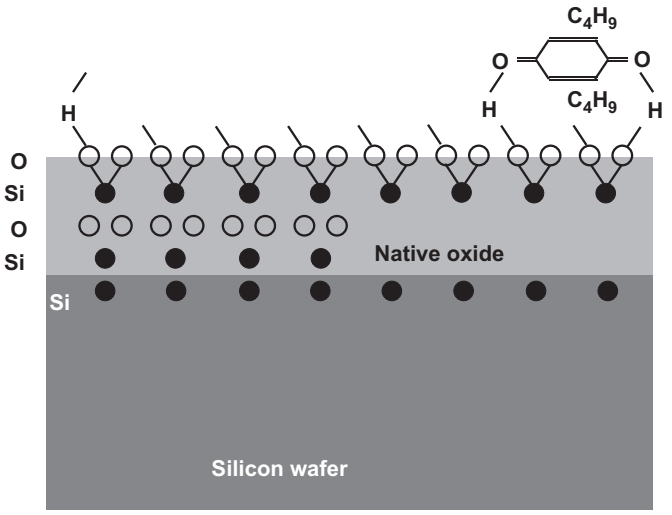

Fig. 4. Model for adsorption of organic contaminants on silicon wafers explaining their removal in sonicated water.

2.3. Wafer material and testing techniques used

The experiments were carried out on commercially available dislocation-free phosphorous doped (n-type, 4.5 Ω cm resistivity) and boron doped (p-type, 10 Ω cm) (1 1 1)-oriented crystalline Cz-silicon wafers with a thickness ranging from 400 to 500 μm. Prior to the intentional contamination, conventional chemical cleaning methods for silicon were used.

Organic contamination was modeled by covering the wafer surface with a thin layer of vaseline (soft paraffin), consisting of chained hydrocarbons and mimicking a hydrocarbon contaminant on Si wafers (Fig. 4) [19]. The contaminating particulates on the Si wafers were detected by measuring Fourier transformed-infrared (FTIR) spectra done with a JASCO 5300 FTIR spectrometer.

Performing current–voltage (I–V) measurements, a barrier contact was formed on the upper surface of the wafer with a gold needle. A GaZn-eutectic forms the Ohmic back contact. The native oxide on the front surface of the wafer was not removed and can only be affected by the exploding bubbles during the acoustic cavitation process. I–V data were recorded by a computerised data acquisition system.

Microindentation hardness (or Vickers hardness, HV) testing is performed with a Vickers Diamond Pyramid indenter PMT-3 (136° between faces, the indentation depth is about 1/7 of the diagonal length). The HV value was calculated from 5 to 10 indentations with a 30 g load. The mean of the two indentation diagonals is used to determine the value of HV with the accuracy of about 4% by dividing the applied load by the surface area of the indentation.

SPV transients are measured in the capacitor arrangement [20], and details of our setup are given elsewhere [21]. The scanning SPV apparatus based on the AC-SPV technique [22] and utilising a "flying spot" arrangement [23] is used for obtaining SPV decays and spatially resolved SPV maps. This technique is capable of providing wafer maps of both the photovoltage size and carrier lifetime with a 100 μm spatial resolution.

3. Results and discussion

3.1. Removal efficiency for organic contaminants

The transmission spectra resulting from the organic contaminants are marked by several peaks in Fig. 5, with C–CH_3 at 2960 cm^{-1}, –CH_2– at 2920 cm^{-1}, –CH at 2890 cm^{-1} and C–H

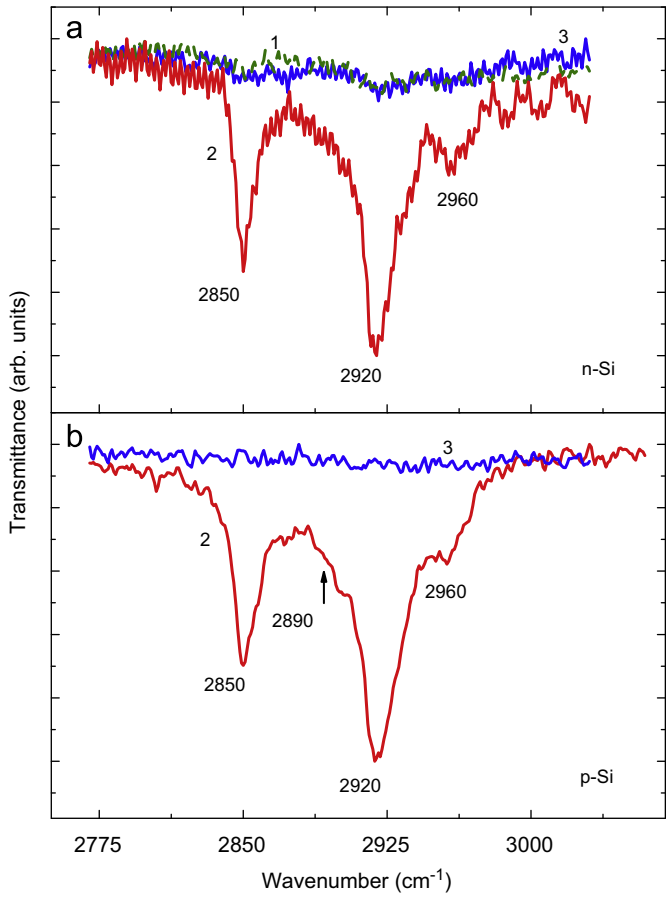

Fig. 5. FTIR spectra of *n*- (a) and *p*-type (b) Si wafers with a surface, conventionally cleaned (1), covered with a thin layer of vaseline (2) and subsequently cleaned in an ultrasonic bath (3) during 15 min.

stretching vibrations [$-CH_3$ and $-(CH_2)_n-$] at 2850 cm^{-1} [24]. The intensity of the peak at 2920 cm^{-1} has a maximum, indicating the presence of $-CH_2-$ stretching vibrations as the predominant group. It is seen from the transmission data that organic contaminants are effectively removed from the wafer surface already at short sonication times (spectra 2 and 3 in Fig. 5) and the transmission with ultrasonically cleaned surface resembles the one with a conventionally cleaned wafer (spectra 3 and 1 in Fig. 5a).

Fig. 4 schematically depicts the dominating monomers and oligomers that are known to dominate the adsorption properties of monolayer organic compounds on silicon surfaces (C_3H_8, C_6H_{14}, C_9H_{20}, $C_{12}H_{26}$, $C_{15}H_{32}$, $C_{18}H_{38}$) [19]. There may be different views on the removal mechanism for organic contaminants. One is that the pressure gradients due to bubble implosion and acoustic streaming would bombard and remove organic contaminants on the silicon surface. The other is that some excited oxygen atoms produced by the sonochemical decomposition of the water adhere to the organic compounds, oxidize them, and finally decompose them into H_2O, O_2, H_2, CO and CO_2, having high vapor pressures allowing the lift-off from the wafer surface.

3.2. Current–voltage characteristics and Vickers hardness

The cleaning processes affect forward and reverse *I–V* characteristics taken in the wafers, as shown in Fig. 6. Here, both sonochemical and chemical cleaning processes are compared utilising distilled water and piranha as a cleaning liquid. It is seen that the overall current through the wafers decreases after the cleanings, which in part may be due to removal of the organic

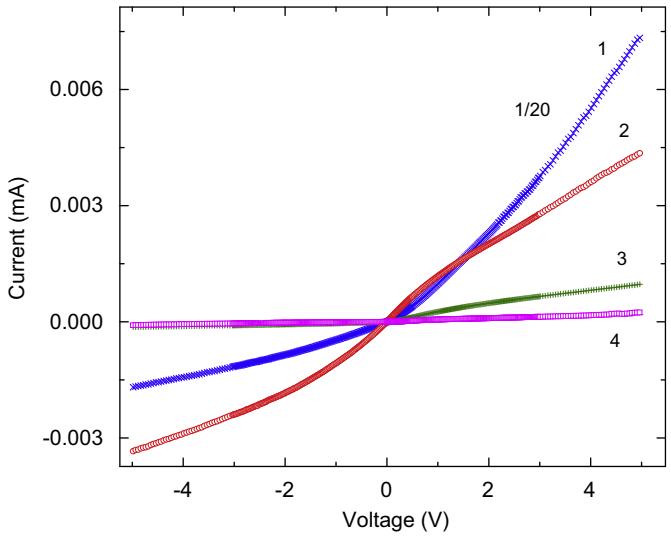

Fig. 6. The reverse and forward *I–V* curves of the Au Schottky contact to *n*-Si, as-purchased (1), ultrasonically cleaned in distilled water (2), processed in a piranha bath (3) and ultrasonically cleaned in a piranha bath (4). The cleaning times are 60 min. Note that points in curve 1 are 1/20 of their measured values.

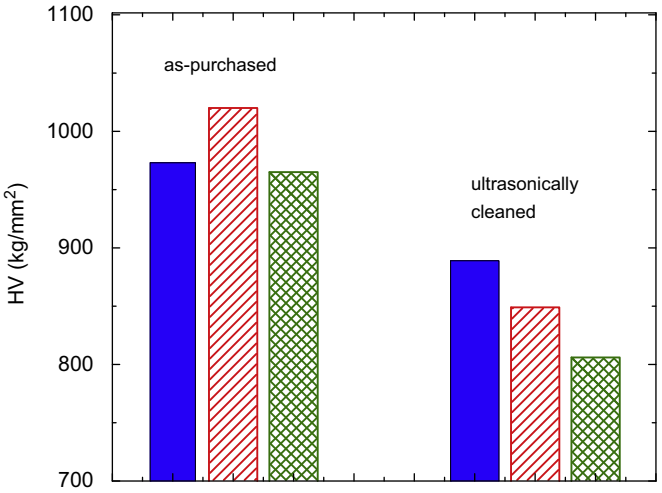

Fig. 7. Vickers hardness of three as-purchased monocrystalline Si wafers (left-hand columns) and of the ones ultrasonically cleaned for 60 min in distilled water (right-hand columns).

contaminants (Section 3.1) with a subsequent quenching of the leaky currents between the upper and bottom wafer surfaces. The effect in the piranha ultrasonic bath is then greater than the one in the water bath (curves 4 and 2 in Fig. 6) because it is known to be highly effective for chemical organic particle removal (curve 3 in Fig. 6).

The wafer sonication also affects the micro-hardness in the subsurface region. Fig. 7 illustrates that the Vickers hardness (HV value) decreases with the water-based cleaning during the first 60 min.

The character of the effect varies with changing processing times, as illustrated in Fig. 8. It is observed that sonicating the wafers for 60–120 min causes a partial recovery of the current towards its initial value (curve 3 in Fig. 8). A similar behaviour of the Vickers hardness was also observed. It was found that, while cleaning over first 40–60 min, the HV value exhibited up to 20% decrease in different samples, whereas the reduction was only 7–11% for longer sonication times.

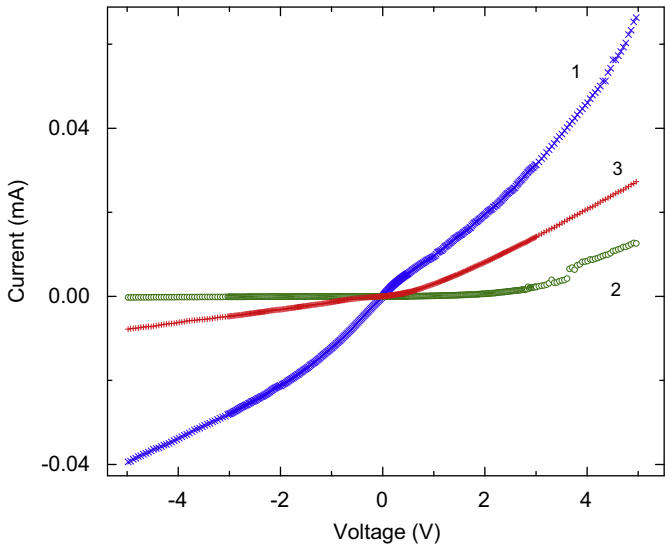

Fig. 8. *I–V* curves of the Au Schottky contact to *n*-Si, as-purchased (1), ultrasonically cleaned in distilled water for 60 (2) and 120 (3) min.

It is well known that the Vickers micro-hardness variations are capable of providing indirect information on the subsurface state through varying mechanical hardness. The fields of elastic tensions caused by cavitation treatments of the wafer surface would extend deep enough inside the wafer to affect both the air/oxide and oxide/wafer interface states. Therefore, it is reasonable to assume that the interface states are modified by the exploding bubbles, which can be credited for some of the features of the cleaning process [25].

Indeed, based on the thermionic emission theory, the current through an ideal Schottky diode is given by [26]

$$I_1 = I_0(e^{qV/kT}-1), \tag{8}$$

where I_0 is the reverse saturation current, q the electronic charge, V the applied bias, T the absolute temperature and k the Boltzmann constant. In the limit of low local state densities, when the energy gap narrowing (ΔE_g) and image force lowering (ΔV_{BF}) are not important, the saturation current is [26]

$$I_0 = AT^2\exp(-qV_{B0}/kT), \tag{9}$$

where A is the effective Richardson constant (112 A cm^{-2} K^{-2} in Si) and V_{B0} is the barrier height for the metal/semiconductor contact. If the gap narrowing and image force lowering are taken into account, the barrier height is modified to become $V_B = V_{B0}-\Delta V_B$, where $\Delta V_B = \Delta E_g/q+\Delta V_{BF}$ is the total barrier height lowering. Taking N_D to be the *n*-doping density, the image force lowering is [27]

$$\Delta V_{BF} \approx \sqrt{\frac{q}{4\pi\varepsilon}}\sqrt{\frac{2qN_D}{\varepsilon}(V+V_{B0})} \tag{10}$$

where ε is the dielectric constant of the wafer. It is evident from Eq. (10) that the greater the doping density, the greater the barrier height lowering due to image force at a fixed value of V.

From the data of Fig. 8, the Schottky barrier heights have been extracted using the techniques described elsewhere [28], showing that the height slightly increases due to the cleaning process (e.g., from 0.69 to 0.75 eV for curves 1 and 2 in Fig. 8). Because the sonication can most probably affect the near-surface region of the wafers, it is likely that cavitating bubbles are capable of modifying the interface dangling bonds, thus modifying the interface charge and consequently increasing the effective defect density represented by N_D in Eq. (10). Another effect may come from the involvement of the sonochemically released oxygen and hydrogen molecules, as discussed later. It can furthermore be implied that the healing of the bonds occurs at longer cleaning times (> 60 min), thus partially reversing the observed changes.

It is of note that, in the discussed case, total current flowing through the metal/semiconductor junction is a combination of the thermionic current and the tunneling current through the interface states. The detailed analysis is even more complicated by introducing the oxide layer between the metal and the semiconductor wafer. Whilst some work on ultrasound effects on *I–V* characteristics of silicon is already done [29–31], the question how much insight into the ultrasound modification of the space-charge regions one may obtain from the *I–V* techniques remains still unanswered.

3.3. Photovoltage performance of the cleaned wafers

The photovoltaic response of silicon wafers is due to the surface band bending. Its time-resolved measurement would therefore be highly sensitive to treatments of the wafer surface occurring in the ultrasonic bath.

The data obtained are exemplified in Fig. 9, illustrating remarkably affected SPV decays due to sonication. Indeed, a remarkable shortening of the SPV decay transients is observed in curve 2 of Fig. 9 compared with curve 1. Within the surface treatment scenario given earlier, the shortening could arise from the dangling bonds created on the bare Si surface due to a local removal of the oxide layer by cavitating bubbles.

At longer sonication times, up to 90–150 min, the wafer performance gradually deteriorates. Thus, the decay curves become double-exponential profiles, developing fast initial decays (cf. at time instants less than 10–20 μs in curve 3 of Fig. 2) and revealing longer ones at greater instants (> 20 μs in curve 3). This fact can be interpreted by the involvement of traps and recombination centers in the near subsurface region. Indeed, the initial decays ($t < 10$ μs), when the injected carrier concentration is large compared with the density of the trapping centers N_t, are governed by the time constant of the recombination centers. Once the injected carrier concentration becomes small compared with N_t ($t > 20$ μs), the decay again is simple exponential determined by N_t. Of importance is the fact that the initial decays observed at ≤ 10 μs in curves 2 and 3 are nearly identical, indicative of a clean wafer surface. Therefore, a subsurface trap generation, referred to as

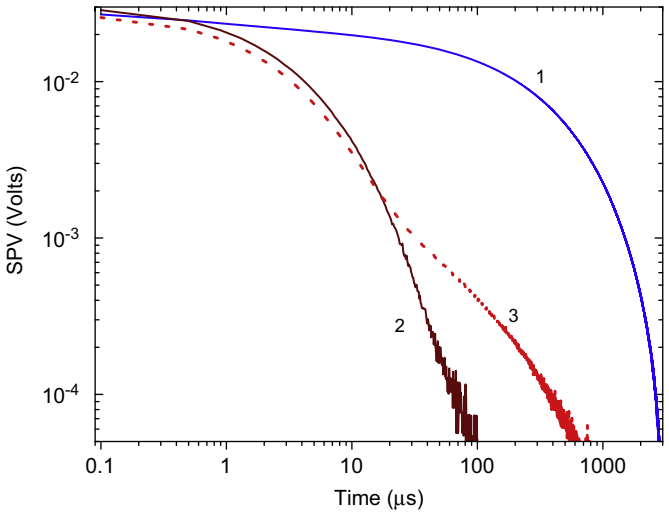

Fig. 9. SPV decays of an *n*-Si wafer, as-purchased (curve 1), ultrasonically cleaned in distilled water for 60 (2) and 120 (3) min.

subsurface damage, is most likely stimulated by elongated (greater than 60–90 min) exposure to the wafer sonication.

3.4. Surface-mapped photovoltage

Since enhanced recombination rate is known to be one of the limiting factors of conversion efficiency of solar cells, the data of Fig. 2 indicate that sonication causes some defects in the wafer subsurface, which deteriorate the carrier lifetime and play a vital role in the wafer degradation. A likely explanation of the enhanced subsurface impurity concentration (revealed, e.g., by the barrier height increase in Section 3.2 and by the shortening of the SPV decay transients in Section 3.3) may come from the oxygen and hydrogen micro-precipitation of the sonicated wafers. It may be assumed that oxygen precipitation would occur due to enhanced oxygen diffusion caused by the presence of local strain fields and elevated temperatures inside a cavitating bubble striking the Si surface. Of further significance may be hydrogen molecules decomposed in water and subsequently trapped at the silicon surface. It is thought that the lattice microdefects present even in high-purity silicon [32–34] would affect the defect reactions with the molecules.

Evidence in order to support this suggestion is deduced by utilising SPV surface scans. Fig. 10 shows the measured decay time maps for as-purchased (*a*) and consequently sonicated (*b*) wafer. The map in (*a*) demonstrates the decay times in the central part of the image are generally higher implying the microdefects, acting like recombination centers, are segregated in the outer regions of image (*a*). The map in (*b*) shows decreased decay times, which is most remarkable in the central part of the image, just in the areas of enhanced times in image (*a*).

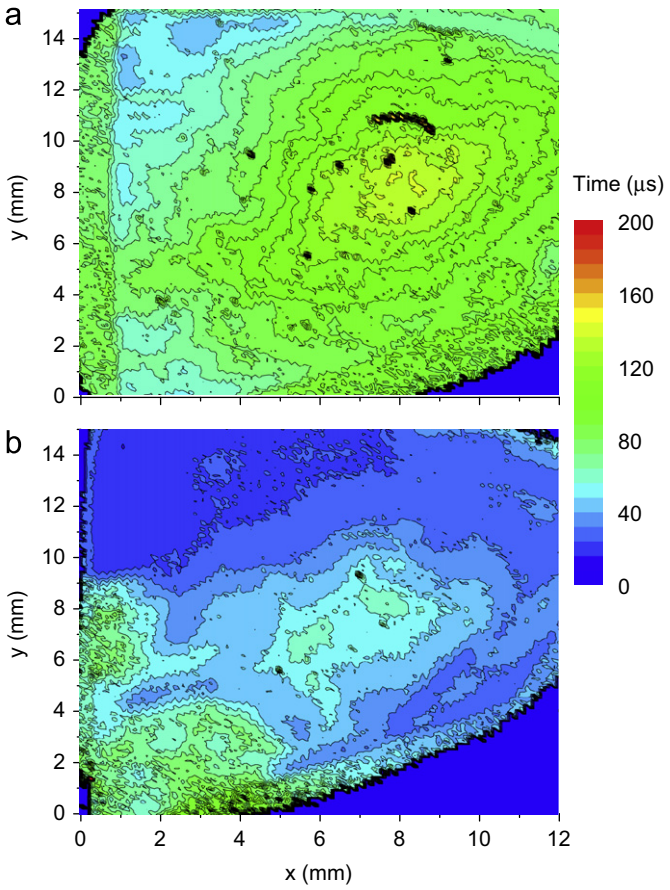

Fig. 10. SPV decay maps of a part of *n*-Si wafer, as-purchased (*a*), and ultrasonically cleaned in distilled water for 60 min (*b*). The decay times were obtained by fitting the initial portion of the decay curves (cf. curves shown in Fig. 9) to the one-exponential form.

It is long believed that there exist several types of microdefects in silicon, which can limit the carrier lifetime in different manners. Thus, A- and B-type defects (microscopic interstitial-type dislocation loops and interstitial-type clusters, respectively) are considered to act as efficient lifetime killers whereas the effect of D- and I-type defects (vacancy clusters and micro-precipitates of trace oxygen, respectively) is much smaller [32–36].

As the defects are distributed non-uniformly in the grown crystals, depending heavily on thermal gradients [32], codoping [34] and many other factors [37], it may be suggested that lifetime killers are segregated in the outer regions of the wafer area depicted in image (*a*) of Fig. 10. Instead, the microdefects, having much less influence on the lifetime, are dominant in the central part of the area imaged in (*a*), thus providing appropriately greater decay times. Then the sonication would act as a driving force for the oxygen and hydrogen micro-precipitation, as discussed earlier.

4. Concluding remarks

Despite the currently insufficient knowledge about the mechanisms taking place during sonication even in distilled water it is of more benefit to delve into the investigation of this class of an environmental friendly cleaning step in silicon wafer preparation. Major progress has recently been made by recognising the unique potential of sonicated water in the various cleaning processes of silicon wafers. The implications on the underlying mechanisms, involved in many of the basic ideas of water sonication techniques, can be quite far reaching and, hence, will stimulate new technologies and, thus, increase our insight into the particular field of silicon cleaning. These new technologies include the fundamental properties of vibrating bubble motions near the solid surface, interbubble interactions and the role of the thin layer between the bubble and the surface in realizing the cleaning effect.

More work needs still to be done beyond the formal description of a very few links that have been highlighted here. In particular, these studies obviously do not reveal the full complexity of subsurface defect distribution effects, so that a number of uncertainties remain, including the fundamental problem of whether or not the environment friendly water cleaning, requiring the acoustic power to be high enough, is capable of promoting sufficient cleaning without deteriorating the wafer performance. Therefore, measures against the deteriorating effects of surface acoustic loads, e.g. decreasing carrier lifetimes, have to be one of the challenges in the future, aiming to find proper ways in exploiting the power of acoustic cleaning techniques.

The following experiments could pave the way for new mechanisms of surface passivation, activation of the interface and grain boundary dangling bonds due to sonication. Several experimental studies that have been reported in the literature provide evidence for involvement of hydrogen atoms and molecules adsorbed at the crystal surface into the surface photovoltage. More work still needs to be done beyond the given description of such links with respect to the surface cleaning in water.

Acknowledgement

This work was supported by the Austrian–Ukrainian Cooperative Agreement no. UA 09/2009 (Mitteln des Bundesministeriums für Wissenschaft und Forschung/Die Österreichische Austauschdienst-GmbH) and no. M/110-2009 (Ministry of Education and Science of Ukraine).

References

[1] S. Wolf, R.N.S. Tauber, Silicon Processing for the VLSI Era, Vol. 1—Process Technology, second ed., Lattice Press, Sunset Beach, CA, 2000, pp. 119–149.
[2] ⟨http://www.itrs.net/⟩.
[3] S.B. Awad, Ultrasonic cleaning mechanism, in: B. Kanegsberg, E. Kanegsberg (Eds.), Handbook for Critical Cleaning, CRC Press, Boca Raton, 2001, pp. 217–227.
[4] A.A. Doinikov, Translational motion of a spherical bubble in an acoustic standing wave of high intensity, Phys. Fluids 14 (2002) 1420–1425.
[5] W.L. Nyborg, in: M.F. Hamilton, D.T. Blackstock (Eds.), Nonlinear Acoustics, Academic, San Diego1998, pp. 207–231 Chap. 7.
[6] G.W. Gale, A.A. Busnaina, Removal of particulate contaminants using ultrasonics and megasonics: a Review, J. Particulate Sci. Technol. 13 (1995) 197–211.
[7] A.A. Busnaina, G.W. Gale, Roles of cavitation and acoustic streaming in megasonic cleaning, J. Particulate Sci. Technol. 17 (1999) 229–238.
[8] W. Kim, T.-H. Kim, J. Choi, H.-Y. Kim, Mechanism of particle removal by megasonic waves, Appl. Phys. Lett. 94 (2009) 081908 (3 pages).
[9] A.A. Busnaina, T.M. Elsawy, Post-CMP cleaning using acoustic streaming, J. Electron. Mater. 27 (1998) 1095–1098.
[10] J.M. Kim, Y.K. Kim, The enhancement of homogeneity in the textured structure of silicon crystal by using ultrasonic wave in the caustic etching process, Sol. Energy Mater. Sol. Cells 81 (2004) 239–247.
[11] J.C. Brice, Crystals for quartz resonators, Rev. Mod. Phys. 57 (1985) 105–147.
[12] P.A. Deymier, A. Khelif, B. Djafari-Rouhani, J.O. Vasseur, Theoretical calculation of the acoustic force on a patterned silicon wafer during megasonic cleaning, J. Appl. Phys. 88 (2000) 2423–2429.
[13] P.A. Deymier, J.O. Vasseur, A. Khelif, S. Raghavan, Second-order sound field during megasonic cleaning of patterned silicon wafers: Application to ridges and trenches, J. Appl. Phys. 90 (2001) 4211–4218.
[14] I. Sokolov, Q.K. Ong, H. Shodiev, N. Chechik, D. James, M. Oliver, AFM study of forces between silica, silicon nitride and polyurethane pads, J. Colloid Interface Sci. 300 (2006) 475–481.
[15] W.C. Hinds, Aerosol Technology, Wiley, New York, 1982, pp. 141–150.
[16] W.D. Kingery, H.K. Bowen, D.R. Uhlmann, Introduction to Ceramics, second ed., Wiley, New York, 1976, pp. 768–816.
[17] F. Shimura, Semiconductor Silicon Crystal Technology, Academic Press, New York, 1989, pp. 228–233.
[18] K.G. Budinski, Engineering Materials, fourth ed., Prentice-Hall, London, 1992, pp. 685–723.
[19] K. Saga, T. Hattori, Identification and removal of trace organic contamination on silicon wafers stored in plastic boxes, J. Electrochem. Soc. 143 (1996) 3279–3284.
[20] C. Munakata, S. Nishimatsu, N. Honma, K. Yagi, Ac surface photovoltages in strongly-inverted oxidized p-type silicon wafers, Jpn. J. Appl. Phys. 23 (1984) 1451–1461.
[21] A. Podolian, V. Kozachenko, A. Nadtochiy, N. Borovoy, O. Korotchenkov, Photovoltage transients at fullerene–metal interfaces, J. Appl. Phys. 107 (2010) 093706 (7 pages).
[22] P. Edelman, J. Lagowski, L. Jastrzebski, Surface charge imaging in semiconductor wafers by surface photovoltage (SPV), Proc. Mater. Res. Soc. Symp. 261 (1992) 223–228.
[23] C. Munakata, K. Yagi, T. Warabisako, M. Nanba, S. Matsubara, Observation of p–n junctions with a flying-spot scanner using a chopped photon beam, Jpn. J. Appl. Phys. 21 (1982) 624–632.
[24] M. Endo, H. Yoshida, Y. Maeda, N. Miyamoto, M. Niwano, Infrared monitoring system for the detection of organic contamination on a 300 mm Si wafer, Appl. Phys. Lett. 75 (1999) 519–521.
[25] A. Nadtochiy, A. Podolian, V. Kuryliuk, A. Kuryliuk, O. Korotchenkov, J. Schmid, V. Schlosser, in: Proceedings of the 27th International Conference on Microelectronics, Niš, Serbia, 2010, IEEE, 2010, pp. 261–264.
[26] S.M. Sze, Physics of Semiconductor Devices, second ed., Wiley, New York, 1982, pp. 245–312.
[27] C.-Y. Nam, D. Tham, P. Jaroenapibal, J. Kim, D.E. Luzzi, S. Evoy, J.E. Fischer, Gallium nitride nanowires: polar surface controlled growth, ohmic contact patterning by focused ion beam induced direct Pt deposition and disorder effects; variable range hopping, and resonant electromechanical properties, Proc. SPIE 6370 (2006) 63701F (12 pages).
[28] D.K. Schroder, Semiconductor Material and Device Characterization, Wiley, New York, 1998, pp. 127–185.
[29] Ya.M. Olikh, M.D. Tymochko, A.P. Dolgolenko, Acoustic-wave-stimulated transformations of radiation defects in γ-irradiated n-type silicon crystals, Tech. Phys. Lett. 32 (2006) 586–589.
[30] N.A. Guseynov, Ya.M. Olikh, Sh.G. Askerov, Ultrasonic treatment restores the photoelectric parameters of silicon solar cells degraded under the action of ^{60}Co gamma radiation, Tech. Phys. Lett. 33 (2007) 18–21.
[31] A.M. Gorb, O.A. Korotchenkov, O.Ya. Olikh, A.O. Podolian, Ultrasonically recovered performance of γ-irradiated metal–silicon structures, IEEE Trans. Nucl. Sci. 57 (2010) 1632–1639.
[32] A.J.R. de Kock, Vacancy clusters in dislocation-free silicon, Appl. Phys. Lett. 16 (1970) 100–102.
[33] T.H. Wang, T.F. Ciszek, T. Schuyler, Micro-defect effects on minority carrier lifetime in high purity dislocation-free silicon single crystals, Sol. Cells 24 (1988) 135–145.
[34] M. Arivanandhan, R. Gotoh, K. Fujiwara, S. Uda, Effects of B and Ge codoping on minority carrier lifetime in Ga-doped Czochralski-silicon, J. Appl. Phys. 106 (2009) 013721 (5 pages).
[35] P.M. Petroff, A.J.R. De Kock, Characterization of swirl defects in floating-zone silicon crystals, J. Cryst. Growth 30 (1975) 117–124.
[36] P.J. Roksnoer, M.M.B. van den Boom, Microdefects in a non-striated distribution in floating-zone silicon crystals, J. Cryst. Growth 53 (1981) 563–573.
[37] H.R. Huff, T. Abe, B.O. Kolbese (Eds.), Electrochemical Society, Pennington, 1986.